**Natural Hazards
and Earth
System Sciences**

Rainfall rate retrieval in presence of path attenuation using C-band polarimetric weather radars

G. Vulpiani[1]**, F. S. Marzano**[1,2]**, V. Chandrasekar**[3]**, A. Berne**[4]**, and R. Uijlenhoet**[4]

[1]Center of Excellence CETEMPS, University of L'Aquila, L'Aquila, Italy
[2]University La Sapienza, Rome, Italy
[3]Colorado State University, Fort Collins, Colorado
[4]Department of Environmental Sciences, Wageningen University, Wageningen, The Netherlands

Abstract. Weather radar systems are very suitable tools for the monitoring of extreme rainfall events providing measurements with high spatial and temporal resolution over a wide geographical area. Nevertheless, radar rainfall retrieval at C-band is prone to several error sources, such as rain path attenuation which affects the accuracy of inversion algorithms. In this paper, the so-called rain profiling techniques (namely the surface reference method FV and the polarimetric method ZPHI) are applied to correct rain path attenuation and a new neural network algorithm is proposed to estimate the rain rate from the corrected measurements of reflectivity and differential reflectivity. A stochastic model, based on disdrometer measurements, is used to generate realistic range profiles of raindrop size distribution parameters while a T-matrix solution technique is adopted to compute the corresponding polarimetric variables. A sensitivity analysis is performed in order to evaluate the expected errors of these methods. It has been found that the ZPHI method is more reliable than FV, being less sensitive to calibration errors. Moreover, the proposed neural network algorithm has shown more accurate rain rate estimates than the corresponding parametric algorithm, especially in presence of calibration errors.

1 Introduction

Radar systems provide rainfall estimates with a high spatial and temporal resolution over extended areas. Such rainfall estimates are crucial for many hydrological applications like (flash) flood forecasting or water resource management (Collier and Knowles, 1986; Wyss et al., 1990; Berenguer et al., 2005). A radar directly measures the reflectivity (related to the dieletric properties of rain), which must be converted into rainfall intensity, the variable of interest for hydrological applications. This conversion introduces uncertainty in radar rainfall estimates (Marzano et al., 2004). The reflectivities at horizontal and vertical polarization measured by polarimetric weather radars provide additional information on the micro-structure of rainfall (Seliga and Bringi, 1976), which can be used to reduce this uncertainty (Bringi and Chandrasekar, 2001).

At wavelengths smaller than 10 cm, the attenuation of the radar signal due to precipitation can be significant and must be compensated in order to use radar rainfall estimates for quantitative applications (Hitschfeld and Bordan, 1954; Hildebrand, 1978; Meneghini et al., 1983; Meneghini and Nakamura, 1990; Iguchi and Meneghini, 1994). As at longer wavelengths (lower frequencies) one needs larger antennæ to achieve the same angular resolution, the cost of a radar system largely depends on its frequency. As a compromise between increased attenuation and reduced cost at shorter wavelengths, most of the European operational weather services have chosen to deploy C-band (about 5 cm wavelength) radar networks.

Regarding these two issues, coherent dual-polarized weather radars represent a unique technological resource, as shown in the recent literature (Bringi and Chandrasekar, 2001), and various approaches have been proposed to exploit Doppler-polarimetric observables for attenuation correction (Gorgucci et al., 1996; Testud et al., 2000; Bringi et al., 2001). In this paper, we focus on two attenuation correction algorithms based on the knowledge of the path integrated attenuation (PIA) at a given range.

Once the reflectivity field has been corrected for attenuation effects, it must be converted to a rainfall intensity field. The main advantage of polarimetric radars is again the possibility to use different types of algorithms, based on polarimetric observables, in order to estimate the rainfall rate (Scarchilli et al., 1993). A new neural network approach to estimate rain rate from the corrected measurements of reflectivity and differential reflectivity is evaluated here.

Correspondence to: G. Vulpiani
(g.vulpiani@aquila.infn.it)

The objective of this paper is to evaluate the performance of the previously mentioned attenuation correction algorithms at C-band in the presence of significant path attenuation and subsequently rainfall at the ground. The neural network approach is applied in cascade to estimate rain rate from corrected polarimetric variables. After a brief overview of the theoretical basis in Sect. 2, range profiles of raindrop size distribution are simulated by using a stochastic model based on disdrometer data (Berne and Uijlenhoet, 2005) while the T-matrix solution technique (Mishchenko, 2000) is adopted to compute the corresponding polarimetric radar observables, as described in Sect. 3. Analysis of model data and numerical tests on synthetic radar data are discussed in Sects. 4 and 5.

2 Theoretical background

A Gamma raindrop size distribution (RSD), having the general form $N(D)=N_0 D^\mu \exp(-\Lambda D)$ with D the particle diameter and N_0, μ and Λ RSD parameters, has been introduced in the literature to account for most of the variability occurring in the naturally observed RSD (Ulbrich, 1983). The multiplication constant N_0, which has units depending on μ (i.e., $mm^{-1-\mu}\,m^{-3}$), is not physically meaningful when $\mu\neq0$. In order to study the underlying shape of the RSD for widely varying rainfall rates, the concept of normalization has been introduced by Willis (1984) and revisited by Chandrasekar and Bringi (1987), Testud et al. (2001), Illingworth and Blackman (2002), and Lee et al. (2004). The number of raindrops per unit volume per unit size can be written as:

$$N(D) = N_w f(\mu)\left(\frac{D}{D_0}\right)^\mu \exp\left[-(3.67+\mu)\frac{D}{D_0}\right] \qquad (1)$$

where $f(\mu)$ is a function of μ only, the parameter D_0 is the median volume drop diameter, μ is the shape of the drop spectrum, and N_w ($mm^{-1}\,m^{-3}$) is a normalized drop concentration that can be calculated as function of liquid water content W and D_0 (Bringi and Chandrasekar, 2001). The shape of a raindrop can be described by an oblate spheroid. The relation between the equivalent spherical volume diameter D (mm) and the raindrop axis ratio r_a (i.e., ratio between the drop minor and major axis) has been investigated by several authors. In this study we limited our attention to the combination (denoted as AB) of that proposed in Andsager et al. (1999)

$$\frac{a}{b} = 1.012 - 10^{-2}(14.45D_e - 10.18D_e^2) \qquad (2)$$

used in the interval $1\,mm \leq D_e \leq 4\,mm$, and that proposed in Chuang and Beard (1990)

$$\frac{a}{b} = 1.005 + 10^{-4}(5.7D_e - 260D_e^2 + 37D_e^3 - 2D_e^4) \qquad (3)$$

for the interval $D_e \leq 1\,mm$, $D_e \geq 4\,mm$.

A raindrop falls with its symmetry axis aligned in the vertical direction. The canting angle in the polarization plane is defined as the angle measured clockwise between the projection of the symmetry axis of a spheroidal particle and the direction running opposite to the vertical. Consequently, in case of horizontal incidence it coincides with the tilt of the particle symmetry axis (Bringi and Chandrasekar, 2001). As shown in Beard and Jameson (1983), the distribution of canting angles can be represented by a Gaussian model with zero mean and standard deviation $\leq 5^o$.

Rainfall rate R, the copolar radar reflectivity factors Z_{hh} and Z_{vv} ($mm^6\,m^{-3}$) at H and V polarization state and the differential reflectivity Z_{dr} [dB] can be expressed as follows:

$$R = 0.6\pi\,10^{-3} \int D^3 N(D) v(D)\,dD \qquad (4)$$

$$Z_{hh,vv} = \frac{\lambda^4}{\pi^5 |K|^2} \langle 4\pi |S_{hh,vv}^b(D)|^2\rangle \qquad (5)$$

$$Z_{dr} = 10\log_{10}\left(\frac{Z_{hh}}{Z_{vv}}\right) \qquad (6)$$

where $S_{hh,vv}$ (mm) are the backscattering co-polar components of the complex scattering matrix **S** of a raindrop, the angular brackets represent the ensemble average over the RSD. K depends on the complex dielectric constant of water estimated as a function of wavelength λ (mm) and temperature (Ray, 1972), and $v(D)$ is the terminal fall speed in still air. As derived by Atlas and Ulbrich (1977), $v(D)$ can be expressed using the following relationship

$$v(D) = 3.78D^{0.67} \qquad (7)$$

For a polarimetric radar, the specific differential phase shift K_{dp}, due to the forward propagation phase difference between H and V polarization and co-polar correlation coefficients ρ_{hv} can be obtained in terms of the scattering matrix **S** as:

$$K_{dp} = 10^{-3}\frac{180}{\pi}\lambda\,Re\big[\langle f_{hh}(D) - f_{vv}(D)\rangle\big] \qquad (8)$$

$$\rho_{hv} = \frac{\langle S_{vv}S_{hh}^*\rangle}{\sqrt{\langle |S_{hh}|^2\rangle\langle |S_{vv}|^2\rangle}} = |\rho_{hv}|e^{j\delta} \qquad (9)$$

where $f_{hh,vv}$ are the forward-scattering co-polar components of **S** and δ (in deg) is the volume backscattering differential phase. The specific attenuation A_{hh} at H polarization and the differential attenuation A_{dp} are finally defined as:

$$A_{hh} = 2\cdot 10^{-3}\lambda\cdot Im\big[\langle f_{hh}(D)\rangle\big], \quad A_{dp} = A_{hh} - A_{vv} \qquad (10)$$

where specific attenuations are in km^{-1}.

3 Simulation of range profiles of Raindrop Size Distribution

The range profiles of RSDs have been generated using a modified version of the stochastic simulator proposed by Berne and Uijlenhoet (2005). It is based on a gamma RSD model (equivalent to Eq. 1 for $\mu=3$):

$$N(D|N_t, \Lambda) = N_t \frac{\Lambda^4}{\Gamma(4)} D^3 e^{-\Lambda D} , \tag{11}$$

where $N(D|N_t, \Lambda)dD$ denotes the drop concentration in the diameter interval $[D, D+dD]$ given N_t (drop concentration) and Λ. The two parameters N_t and Λ are assumed to be random variables, jointly lognormally distributed. To introduce a spatial structure in the profiles, $N'=\ln N_t$ and $\Lambda'=\ln \Lambda$ are assumed to follow a first order discrete vector auto-regressive process. This results in an exponential auto-correlation function:

$$\rho(r) = e^{-2r/\theta} , \tag{12}$$

where r represents the distance lag and θ the characteristic spatial scale, also known as the scale of fluctuation:

$$\theta = 2 \int_0^{+\infty} \rho(r) dr . \tag{13}$$

The stochastic simulator is able to produce range profiles of RSDs of equivolumetric spherical drops.

RSD time series measurements from an optical spectropluviometer, collected during the HIRE'98 experiment (Uijlenhoet et al., 1999) in Marseille, France, are used to parameterize the simulator. To simulate strong rain events, we focus on a period of 45 min of intense rainfall during the 7 September 1998 rain event. Assuming Taylor's hypothesis with a constant velocity of $12.5\,\text{m s}^{-1}$, consistent with the wind speed estimate of Berne et al. (2004), the required spatial characteristics of N' and Λ' can be derived. To achieve a high spatial resolution of 250 m, RSD data have been analyzed at 20 s. The total length of the profiles is fixed to 80 km. The analysis of the fitted N' and Λ' values shows that the cross-correlation is negligible. The number of model parameters now reduces to five: the mean and standard deviation of N' and Λ', and the characteristic scale θ (assumed to be equal for N' and Λ'). Their values are given in Table 1. A total number of 100 profiles of RSD parameters have been generated. Figure 1 shows an example of stochastically generated range profile of N_w and D_0 and the corresponding ones of reflectivity and rain rate. Once a RSD is defined, the polarimetric radar parameters can be computed from the equations given in Sect. 2. Numerically computed forward scatter and backscatter amplitudes of raindrops for a given size are used to derive the radar parameters for a given RSD (Mishchenko, 2000). Computations are carried out at C-band

Table 1. Mean, standard deviation and characteristic time of $N'=\ln N_t$ (with N_t in m^{-3}) and $\Lambda'=\ln \Lambda$ (with Λ in mm^{-1}) deduced from HIRE'98 data (45 min intense rainfall period of the 7 September 1998 event) at a 4 s time step.

	Mean	Std	θ (m)
N'	6.30	0.58	3200
λ'	1.3	0.32	3200

and the Gamma RSD is assumed for raindrop diameters between 0.5 and 8 mm. Figure 2 shows the statistics of the simulated RSD parameters (upper panels) and the corresponding rain rate (lower panel). The simulated rain rate values range from $0.1\,\text{mm h}^{-1}$ to $143\,\text{mm h}^{-1}$ with $\bar{R}=7.8\,\text{mm h}^{-1}$ and $\sigma_R=8.7\,\text{mm h}^{-1}$. About 49% of the whole data set is characterized by rain rate values less than $5\,\text{mm h}^{-1}$, and R ranges in the interval $5<R<25\,\text{mm h}^{-1}$ in about 47% of the cases.

Figure 3 shows the scatterplot of Z_{dr} vs. Z_{hh}, A_{hh} vs. Z_{hh}, K_{dp} vs. Z_{hh} and A_{hh} vs. K_{dp} at C band. Amplitude variables are expressed in dB. The values of Z_{hh} vary up to 58 dBZ and those of Z_{dr} up to 4.5 dB. It is interesting to note the dominant linear correlation between the specific differential phase and the specific attenuation, even though a non negligible variance is appreciable for values of K_{dp} larger than $5°\,\text{km}^{-1}$.

4 Rain path attenuation correction

4.1 Rain profiling algorithms

Since the beginning of radar meteorology, many techniques have been proposed to correct radar measurements for rain path attenuation. The iterative approaches (Hitschfeld and Bordan, 1954; Hildebrand, 1978), beginning from the closest (to the radar) range resolution volume and proceeding to farther (successive) resolution volumes, are known to be unstable and sensitive to potential radar calibration error. A significant improvement to these path-attenuation correction procedures is provided by using the total path-integrated attenuation (PIA) as a constraint. These approaches (called rain profiling algorithms), originally proposed for spaceborne radar applications where the sea or land surface is generally assumed as a reference target, have been extended to ground-based polarimetric radar. Recently, the use of a cumulative differential phase (Φ_{dp}) constraint to estimate the PIA and to correct the measured reflectivity Z_{hh} and differential reflectivity Z_{dr}, proposed and evaluated by Testud et al. (2000) and Le Bouar et al. (2001) respectively, was improved by Bringi et al. (2001) through the use of a self-consistent scheme.
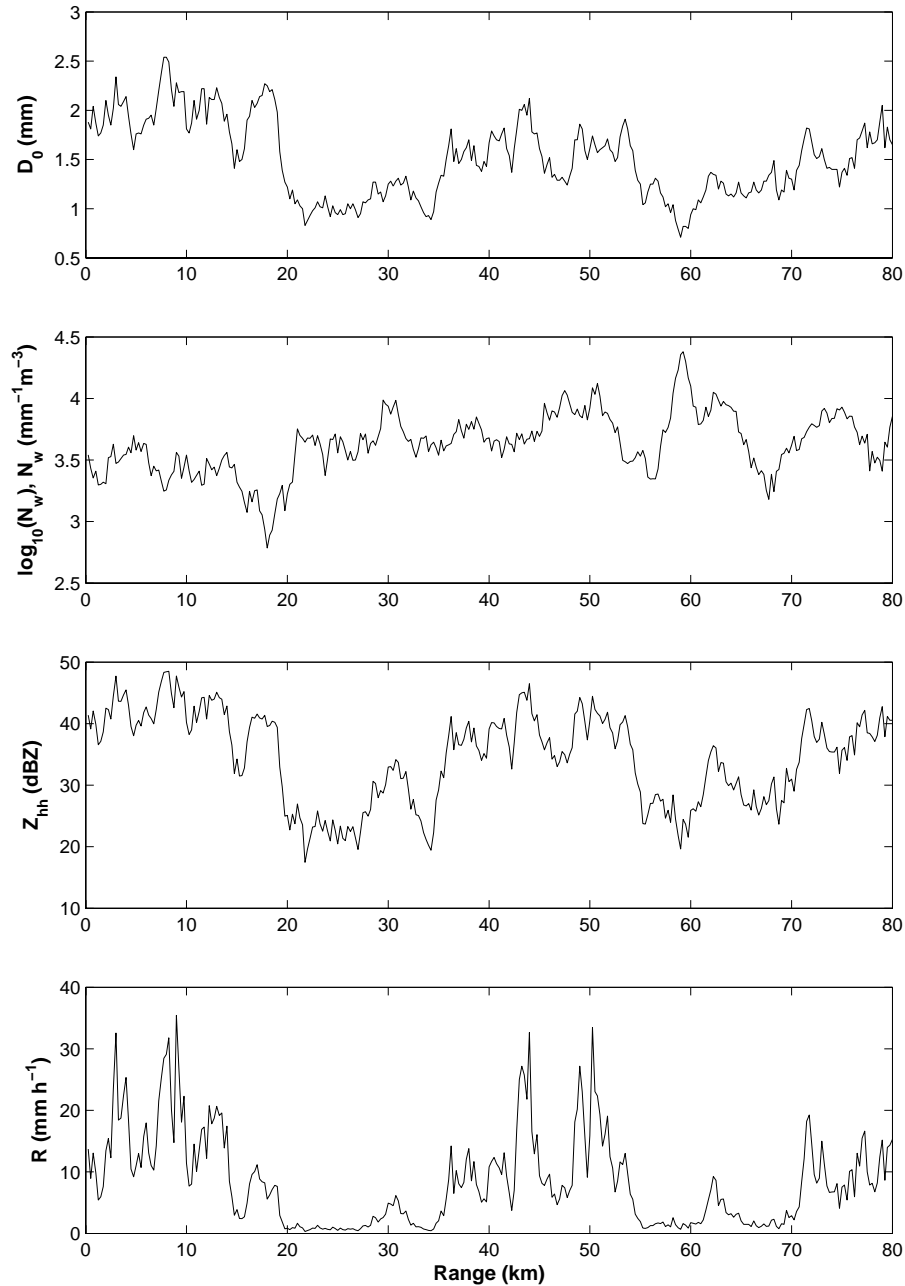
Fig. 1. A stochastically generated range profile of RSD parameters and the corresponding ones of reflectivity and rain rate.

In this section we will briefly resume the polarimetric constrained techniques, whereas their detailed derivation can be found in Appendix A. In the presence of path attenuation, the measured copolar reflectivity $Z_{hh\,m}$ can be written as

$$10\log_{10}(Z_{hh\,m}(r)) = 10\log_{10}(Z_{hh}(r)) - 2\int_{r_0}^{r} A_{hh}(s)\,ds \quad (14)$$

where r is the range and r_0 is the rain range bin closest to the radar or, in general, the initial range of the considered rain segment.

The rain profiling algorithms are constrained solutions to the differential equation which can be obtained from Eq. (14) when the specific attenuation A_{hh} (expressed in dB km^{-1}) is assumed to be related to the horizontally polarized reflectivity Z_{hh} (expressed in mm^6 m^{-3}) through a power law $A_{hh} = \alpha Z_{hh}^{\beta}$ with β assumed constant in range. When the constraint is assumed at the farthest range bin (i.e., the estimated path integrated attenuation at $r = r_n$ is used as constraint) the so-called Final Value (FV) (i.e., Meneghini et al., 1983, 1992; Meneghini and Nakamura, 1990) is obtained
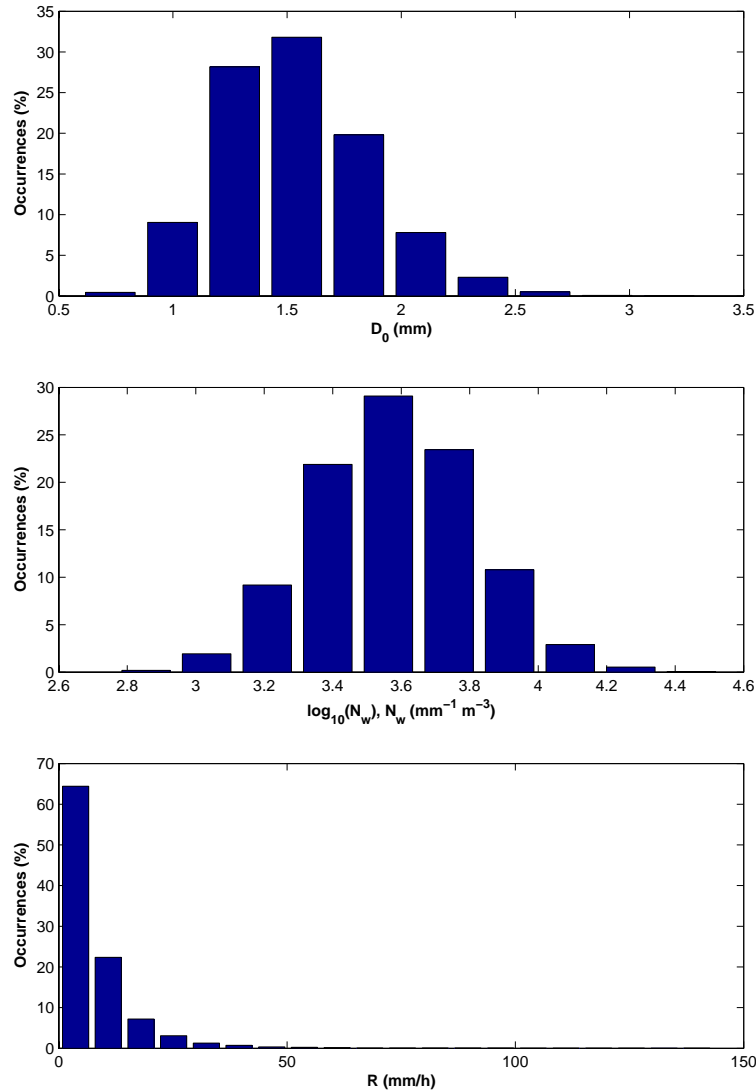
Fig. 2. Histograms of the simulated RSD parameters and the corresponding rain rate.

$$A_{hh}^{(FV)}(r) = \frac{\alpha(r)\left[Z_{hh\,m}(r)\right]^{\beta}}{A_f^{\beta} + S(r_n) - S(r)} \tag{15}$$

where $S(r) = q \int_{r_0}^{r} \alpha Z_{hh\,m}(s)^{\beta}\,ds$, $q = 0.2\,\beta\,\ln(10)$ and $A_f = \exp\left[-0.46 \int_{r_0}^{r_n} A_{hh}(s)\,ds\right]$.

Otherwise, if the constraint is applied also to the first range bin (i.e., $Z_{hh\,m}(r_0) = Z_{hh}(r_0)$) and α is assumed constant in range, the CA solution (Meneghini et al., 1983; Meneghini and Nakamura, 1990) assumes the following form

$$A_{hh}^{(CA)}(r) = \frac{\left[Z_{hh\,m}(r)\right]^{\beta}\left(A_f^{-\beta} - 1\right)}{I(0, r) + \left(A_f^{-\beta} - 1\right) I(r, r_n)} \tag{16}$$

where $I(r, r_n) = q \int_{r}^{r_n} \left[Z_{hh\,m}(s)\right]^{\beta}\,ds$.

When the differential phase measurements are used to estimate the constraint at the farthest range bin, as proposed in Testud et al. (2001), Eq. (16) coincides with the so-called ZPHI algorithm (see Appendix A for more details). In this work, the same approach has been followed to constrain the FV solution.

As outlined in Bringi et al. (2001), the approach to estimate the path integrated attenuation through Φ_{dp} is temperature dependent. To overcome this problem a self-consistent technique has been proposed in Bringi et al. (2001). It is worth mentioning that the same approach can be followed to derive the specific differential attenuation A_{dp} as a function of differential reflectivity Z_{dr}. In order to compare the performance of the various profiling algorithms (FV, CA (ZPHI)) the same optimized Φ_{dp} constraint has been applied in the present work.
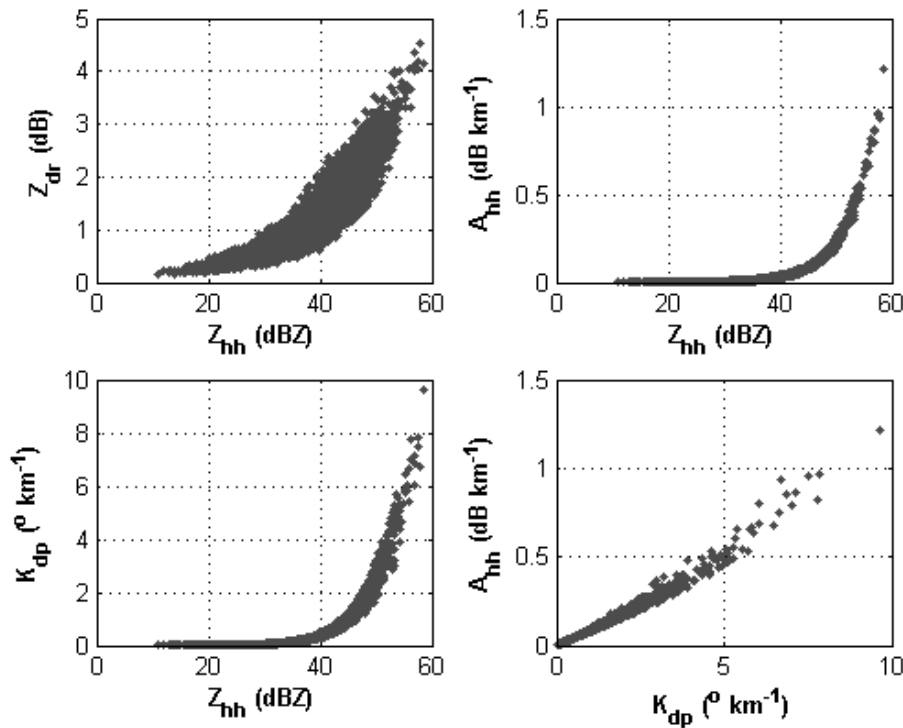
Fig. 3. Scatterplot of Z_{dr} vs. Z_{hh}, A_{hh} vs. Z_{hh}, K_{dp} vs. Z_{hh} and A_{hh} vs. K_{dp} at C band. Amplitude variables are expressed in dB.

Table 2. Reflectivity correction. Error statistics in absence of calibration error.

Algorithm	$\bar{\epsilon}$ (dB)	σ_ϵ (dB)	RMSE (dB)
ZPHI	0.07	0.91	0.92
FV	−0.05	0.86	0.86

4.2 Numerical results

The results, obtained by applying the mentioned rain profiling algorithms (ZPHI, FV) to the synthetic data set described in Sect. 3, are discussed here. For the sake of brevity we limit our treatment to the case of the Z_{hh} correction, the corresponding Z_{dr} case being qualitatively similar. The error analysis has been accomplished in terms of mean error ($\bar{\epsilon}$), error standard deviation (σ_ϵ) and root mean square error (RMSE=$\sqrt{\bar{\epsilon}^2+\sigma_\epsilon^2}$) computed as a function of range for all profiles. In this work the error is defined as

$$\varepsilon(r) = 10 \log_{10}(\hat{Z}(r)) - 10 \log_{10}(Z(r)) \qquad (17)$$

where $\hat{Z}(r)$ indicates the estimate of the attenuation-corrected radar reflectivity while $Z(r)$ is the true (simulated) reflectivity.

Figure 4 shows the histograms of $\bar{\epsilon}$ and σ_ϵ obtained in absence of calibration errors. The same error indicators together with the RMSE, calculated for the whole simulated

data set, are shown in Table 2. From Fig. 4 and Table 2 it can be noticed that the performance of the two profiling algorithms is essentially similar. In the absence of calibration errors, the FV algorithm performs slightly better than ZPHI both in terms of $\bar{\epsilon}$ and σ_ϵ, with RMSE=0.92 dB for ZPHI and RMSE=0.86 dB for FV. This behavior could be attributed to the range variability of N_w assumed constant in the ZPHI algorithm. In order to test the robustness of the mentioned algorithms, a sensitivity analysis with respect to calibration errors is also performed. As a matter of fact, systematic errors on Z_{hh} and Z_{dr} can affect both the attenuation compensation and the rainfall retrieval algorithms. Typically in a well-maintained radar the error bias on Z_{dr} is less than 0.2 dB while the bias on Z_{hh} is less than 1 dBZ. The bias on differential reflectivity can be estimated and removed in a fairly easy way (Gorgucci et al., 1999), because it is a differential power measurement. However, it is difficult to obtain the absolute calibration of Z_{hh}. For this reason, assuming a bias of 0.2 dB on Z_{dr}, we focused on the impact that the error bias on Z_{hh} has on the examined path-attenuation correction techniques. As expected, the results change when the calibration error is added (see Fig. 5 and Table 3), being RMSE=1.38 dB for ZPHI and RMSE=1.43 dB for FV. The increase of RMSE is a consequence of the increasing mean error (about 1 dB, comparable to the calibration error), the standard deviation remaining substantially unaltered. In that case the ability to adjust the radar constant makes ZPHI more reliable than FV.
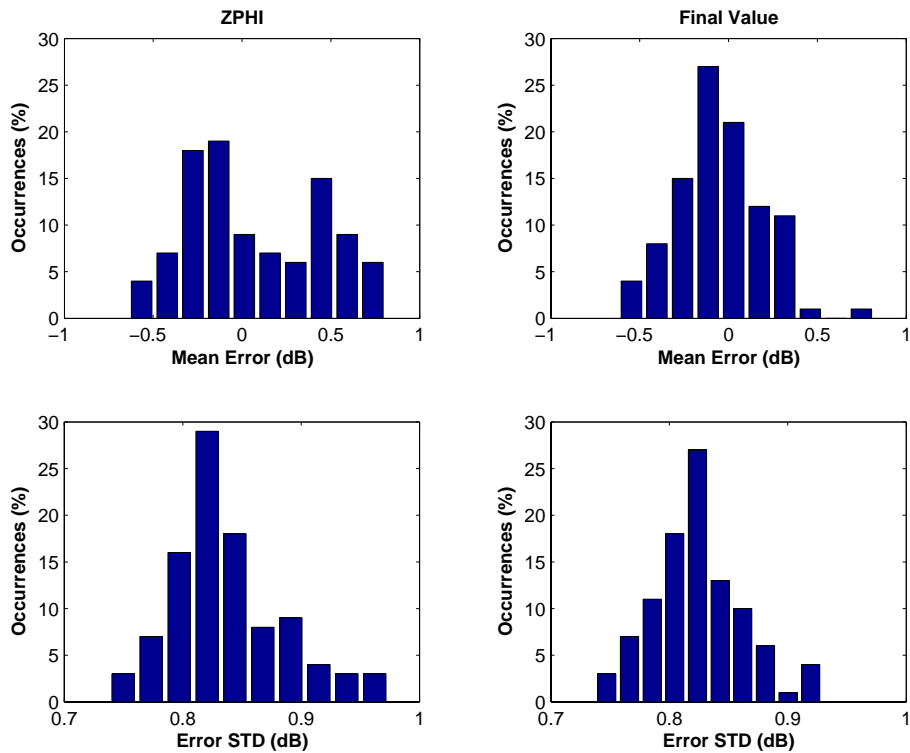
Fig. 4. The performance of ZPHI (left panels) and FV (right panels) are compared in terms of the histogram of $\bar{\varepsilon}$ and σ_ε computed for each range profile realization in absence of calibration errors.
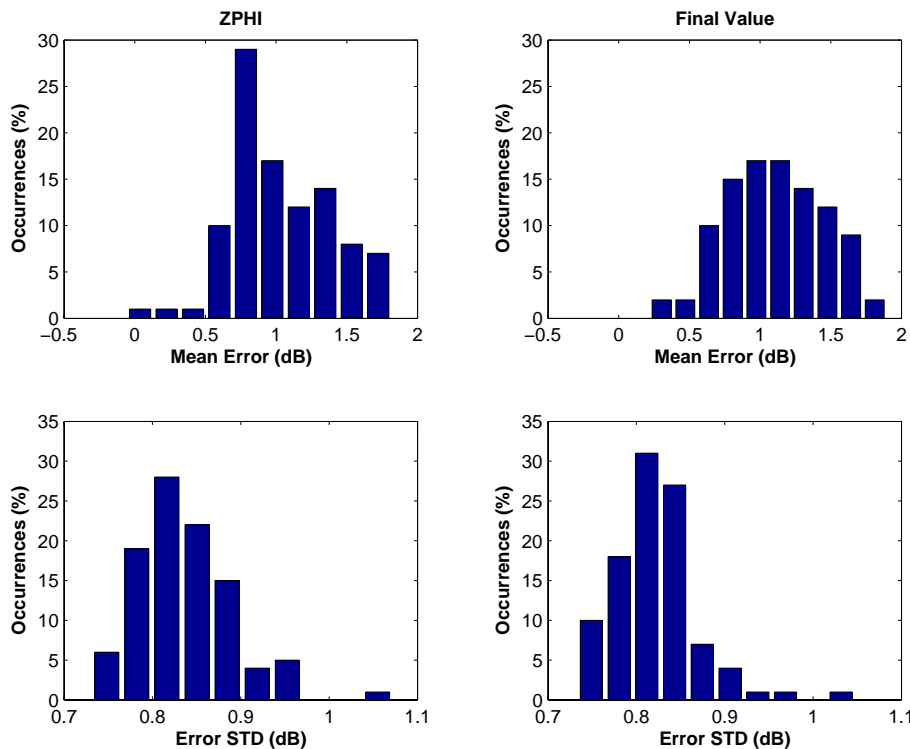

Fig. 5. As in Fig. 4 but assuming a calibration error of 1 dB on Z_{hh} and 0.2 dB on Z_{dr}.

Table 3. Reflectivity correction. Error statistics in presence of calibration error.

Algorithm	$\bar{\epsilon}$ (dB)	σ_ϵ (dB)	RMSE (dB)
ZPHI	1.04	0.91	1.38
FV	1.11	0.90	1.43

5 Rain rate retrieval

In addition to the classical $R(Z_{hh})$ rain rate retrieval algorithm, polarization diversity allows to employ the two parameter algorithms $R(Z_{hh}, Z_{dr})$ and $R(Z_{dr}, K_{dp})$ as well as $R(K_{dp})$ (Scarchilli et al., 1993; Gorgucci et al., 1996). The algorithms using reflectivity and differential reflectivity are affected by radar calibration errors. On the other hand, those using the K_{dp} are conditioned by the differentiation scheme adopted to derive it from Φ_{dp}, which is also contaminated by the backscattering differential phase. As a consequence, none of these techniques is completely satisfactory. Neural networks represent a powerful tool for non-linear inverse problems and they have already been applied to rain rate estimation from radar data (e.g., Bringi and Chandrasekar, 2001; Marzano et al., 2004). A topology with an input, a hidden and an output layer, has been shown to approximate a non-linear function to any degree of non linearity (Haykin, 1995). In this section, a rain rate retrieval algorithm based on such a neural network is presented and its performance compared with that of a parametric algorithm (Bringi and Chandrasekar, 2001).

5.1 Rain rate algorithms

The rainfall estimator proposed in this work, indicated as $R_{NN}(Z_{hh}, Z_{dr})$, is based on a feed-forward neural network with a back-propagation learning algorithm and uses the retrieved corrected profiles of Z_{hh}, Z_{dr}. In a formal way, we can write:

$$R_{NN} = NN_R(Z_{hh}, Z_{dr}) \tag{18}$$

where NN_R is a Neural Network estimator used for the rain rate estimation (Marzano et al., 2004). A multi-layer feed-forward neural network, characterized by a back-propagation learning rule, an input layer and an output layer, was implemented in this work. A 4-layer neural network, composed by an input layer, two hidden layers and an output layer, was chosen for its simplicity and effectiveness. The number of input nodes was set to two, while the number of output nodes was set to 1. After an optimization process, called "neural network pruning", the number of nodes in the hidden layers was chosen equal to 4 and 3 respectively (see Fig. 6). In order to generate a large training data set, we adopted for D_0 and μ a uniform distribution inside the range proposed by Chandrasekar and Bringi (1987), that is $0.5 \leq D_0 \leq 3.5$ mm
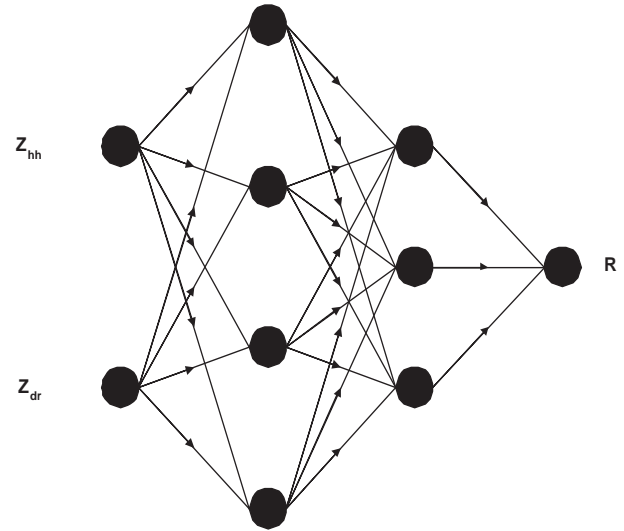

Fig. 6. Architecture of the Neural Network used to estimate the rainfall rate. A 4-layer neural network, composed of an input layer, two hidden layers and an output layer was chosen for its effectiveness. The number of nodes in the hidden layers was chosen equal to 4 and 3 respectively.

and $-1 < \mu \leq 5$. N_w has been generated by assuming a random distribution of water content W which results in a variability of rain rate from 0 to 300 mm h^{-1}. Temperatures of raindrops have been varied between 5°C and 30°C with a step of 5°C. We are assuming here the most widely varying RSD parameters without any correlation among them in order to ensure the training of the retrieval algorithm even in the most general conditions.

As a comparison, the parametric algorithm given in Bringi and Chandrasekar (2001)

$$R_{DR} = 5.1 \times 10^{-3} Z_{hh}^{0.91} 10^{-2.09 Z_{dr}} \tag{19}$$

has been adopted for making comparisons with the neural network rainfall estimates based on Z_{hh} and Z_{dr}.

5.2 Numerical results

After applying the attenuation correction algorithms, the corrected values of Z_{hh} and Z_{dr} are used to estimate the rain rate through the R_{NN} and R_{DR} algorithms described in the previous section. The mentioned rain rate estimators are evaluated using the same error indicators as in Sect. 4.2. Figure 7 shows the histograms of $\bar{\epsilon}$, σ_ϵ obtained applying the neural network based rain rate algorithm to the profiles of Z_{hh}, Z_{dr} corrected by both ZPHI and FV. The same errors computed for the whole data set, are listed in Table 4 for each examined rain profiling algorithm and rainfall retrieval technique. Assuming a well calibrated radar system, $\bar{\epsilon}$ is less than 0.6 mm h^{-1} while σ_ϵ is less than 4 mm h^{-1}, using the R_{NN} technique independent of the attenuation correction algorithm. The results obtained applying the parametric
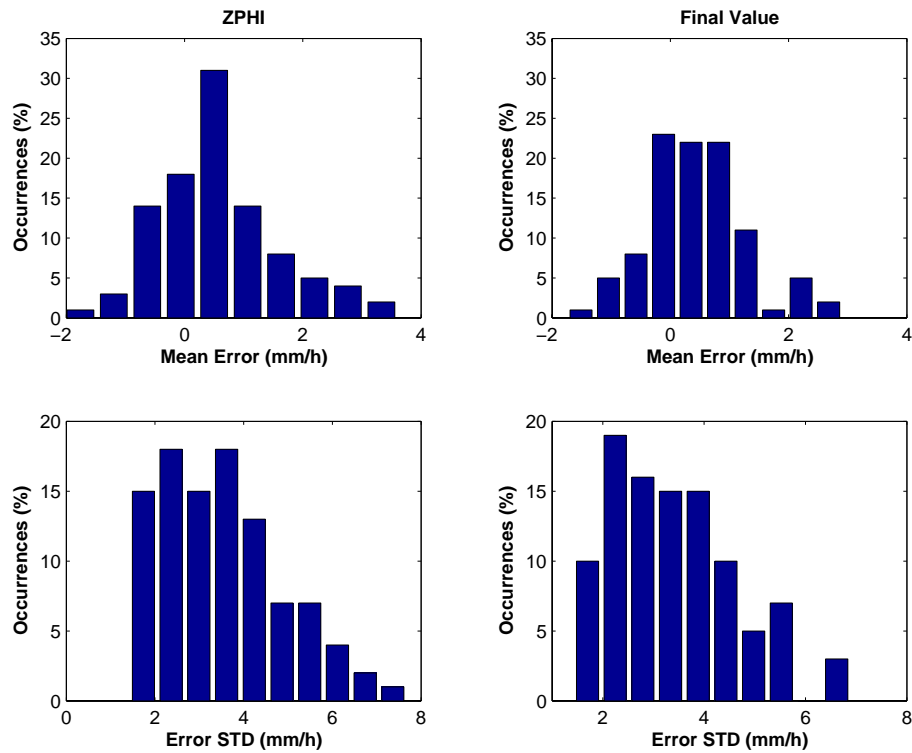
Fig. 7. Performance of the neural network based rainfall rate retrieval algorithm in terms of the histogram of $\bar{\varepsilon}$ and σ_ε computed for each range profile realization in absence of calibration error. The rainfall algorithm is applied to the profiles of Z_{hh} and Z_{dr} corrected using ZPHI (left panels) and FV (right panels), respectively.

Table 4. Rainfall rate retrieval. Error statistics in absence of calibration error.

Rain rate algorithm	Rain profiling algorithm	$\bar{\epsilon}$ (mm h^{-1})	σ_ϵ (mm h^{-1})	RMSE (mm h^{-1})
R_{NN}	ZPHI	0.58	3.90	3.94
R_{NN}	FV	0.43	3.71	3.74
R_{DR}	ZPHI	1.89	4.83	5.20
R_{DR}	FV	1.69	4.61	4.91

Table 5. Rainfall rate retrieval. Error statistics in presence of calibration error.

Rain rate algorithm	Rain profiling algorithm	$\bar{\epsilon}$ (mm h^{-1})	σ_ϵ (mm h^{-1})	RMSE (mm h^{-1})
R_{NN}	ZPHI	1.73	4.87	5.17
R_{NN}	FV	1.88	5.12	5.46
R_{DR}	ZPHI	3.45	6.52	7.37
R_{DR}	FV	3.64	6.87	7.78

algorithm R_{DR} are characterized by bigger mean error and error standard deviation. The resulting RMSE is increased by more than 1 mm h^{-1} with respect to the R_{NN} case. Finally, it can be seen from Fig. 8 and Table 5 that the calibration errors impact more the parametric than the neural network algorithm, the difference in RMSE being increased by more than 2 mm h^{-1}.

6 Conclusions

Weather radar systems allow the monitoring of rainfall events, representing a powerful tool for meteorological and hydrological purposes. Quantitative precipitation estimates are prone to several error sources which affect the accuracy of inversion algorithms. These uncertainties can be reduced by using coherent dual-polarized radar systems and suitable correction algorithms. In this paper, we concentrate on one such source of error, namely the rain path attenuation. The most advanced attenuation correction procedures (called rain profiling algorithms) have been compared. The relative performance of these techniques is evaluated on the basis of rain rate retrievals produced by a new neural network inversion algorithm and a parametric algorithm. For this purpose, a stochastic model, based on disdrometer measurements, is used to generate realistic range profiles of
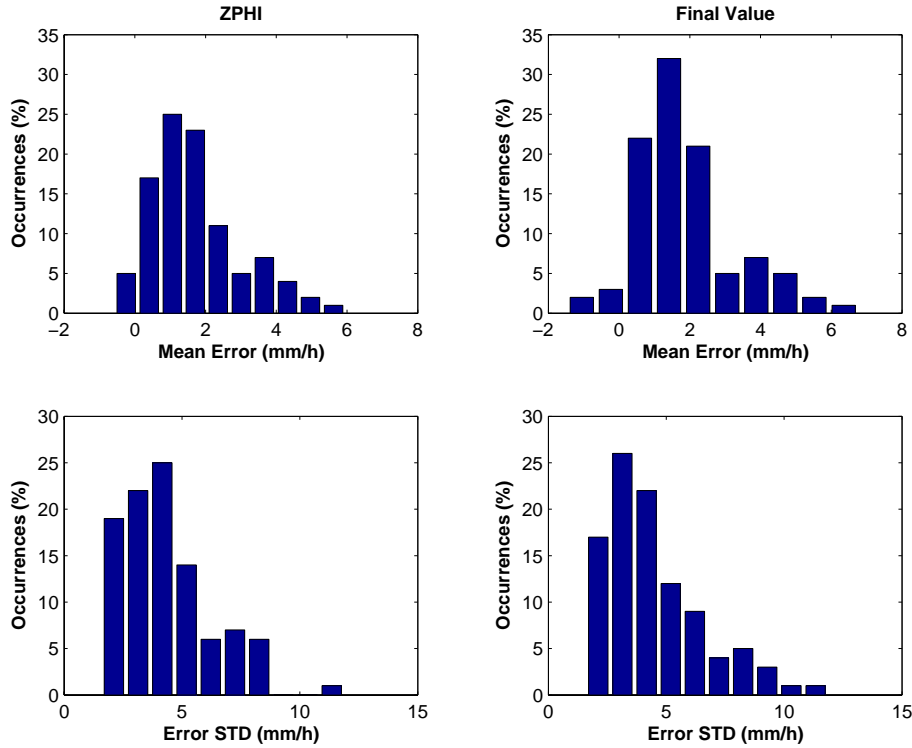
Fig. 8. As in Fig. 7 but assuming a calibration error of 1 dB on Z_{hh} and 0.2 dB on Z_{dr}.

raindrop size distribution parameters, while a T-matrix solution technique is adopted to compute the corresponding polarimetric variables. Numerical results have shown that FV performs slightly better than ZPHI when calibration errors can be neglected, otherwise the latter is more reliable. Moreover, it has been found that the neural network based rainfall retrieval algorithm, in spite of its greater complexity, produces more accurate rainfall estimates than the corresponding parametric algorithm (independent of the applied attenuation correction technique), especially in presence of calibration errors.

Appendix A

Rain profiling algorithms

A detailed derivation of the so-called profiling techniques for attenuation correction is given in this appendix.

When attenuation occurs, the measured reflectivity at horizontal polarization ($Z_{hh\,m}$) can be written as

$$Z_{hh\,m}(r) = Z_{hh}(r) \exp\left[-0.46 \int_{r_0}^{r} A_{hh}(s)\,ds \right] \qquad (A1)$$

where the specific attenuation A_{hh} (expressed in dB km^{-1}) is assumed to be related to the horizontally polarized Z_{hh}

(expressed in mm^6 m^{-3}) through a power law,

$$A_{hh} = \alpha Z_{hh}^{\beta} \qquad (A2)$$

Assuming β is constant in range, Eq. (A1) can be rewritten as a differential equation (Meneghini et al., 1992) which takes the form of a Riccati differential equation (Abramowitz and Stegun, 1972). A general solution to this differential equation is

$$Z_{hh}(r) = Z_{hh\,m}(r)\left[C_1 - S(r)\right]^{-1/\beta} \qquad (A3)$$

where $S(r) = q \int_{r_0}^{r} \alpha Z_{hh\,m}(s)^{\beta}\,ds$ and $q = 0.2\,\beta\,\ln(10)$. It is worth mentioning that the same approach can be followed to derive the specific differential attenuation A_{dp} as a function differential reflectivity Z_{dr}. If $Z_{hh}(r_0) = Z_{hh\,m}(r_0)$ is taken as a boundary condition, then the Hitschfeld-Bordan (HB) solution is obtained (Hitschfeld and Bordan, 1954)

$$Z_{hh}^{(HB)}(r) = Z_{hh\,m}(r)\left[1 - S(r)\right]^{-1/\beta} \qquad (A4)$$

$$A_{hh}^{(HB)}(r) = \frac{\alpha\left[Z_{hh\,m}(r)\right]^{\beta}}{1 - S(r)} \qquad (A5)$$

In order to avoid the instability of the solution, the boundary condition at the farthest range bin ($r = r_n$) can be applied to constrain the solution. Defining the attenuation factor A_f as

$$A_f = \exp\left[-0.46 \int_{r_0}^{r_n} A_{hh}(s)\,ds \right] \qquad (A6)$$

it is possible to derive the so-called final-value (FV) solution

$$Z_{hh}^{(FV)}(r) = Z_{hh\,m}(r)\Big[A_f^{\beta} + S(r_n) - S(r)\Big]^{-1/\beta} \qquad (A7)$$

$$A_{hh}^{(FV)}(r) = \frac{\alpha(r)\Big[Z_{hh\,m}(r)\Big]^{\beta}}{A_f^{\beta} + S(r_n) - S(r)} \qquad (A8)$$

It is known that the HB solution can become unstable in heavy rain. The FV solution, on the other hand is stable using the path-integrated attenuation (PIA) as boundary condition. To satisfy both the initial and PIA conditions, the constant adjustment (CA) method proposed in Meneghini et al. (1983) was modified by Meneghini and Nakamura (1990) who adjust the radar constant introducing the correction factor $\varepsilon = \frac{1 - A_f^{\beta}}{S(r_n)}$. The CA solution is given by:

$$Z_{hh}^{(CA)}(r) = \varepsilon^{1/\beta} Z_{hh\,m}(r)\Big[1 - \varepsilon S(r)\Big]^{-1/\beta}$$
$$= Z_{hh\,m}(r)\left\{\frac{A_f^{\beta}}{\varepsilon} + \Big[S(r_n) - S(r)\Big]\right\}^{-1/\beta} \qquad (A9)$$

$$A_{hh}^{(CA)}(r) = \frac{\alpha(r)\Big[Z_{hh\,m}(r)\Big]^{\beta}\Big[1 - A_f^{\beta}\Big]}{A_f^{\beta} S(r_n) + \Big(1 - A_f^{\beta}\Big)\Big[S(r_n) - S(r)\Big]}$$
$$= \frac{\alpha(r)\Big[Z_{hh\,m}(r)\Big]^{\beta}\Big(A_f^{-\beta} - 1\Big)}{S(r_n) + \Big(A_f^{-\beta} - 1\Big)\Big[S(r_n) - S(r)\Big]} \qquad (A10)$$

Note that if α is constant in range the above equation can be rewritten as

$$A_{hh}^{(CA)}(r) = \frac{\Big[Z_{hh\,m}(r)\Big]^{\beta}\Big(A_f^{-\beta} - 1\Big)}{I(0, r) + \Big(A_f^{-\beta} - 1\Big) I(r, r_n)} \qquad (A11)$$

where $I(r, r_n) = q \int_r^{r_n} [Z_{hh\,m}(s)]^{\beta}\, ds$. The above profiling techniques (FV, CA), also called surface reference methods, estimate the PIA through rain from the decrease in surface return; in particular the loss factor A_f at $r = r_n$ is estimated as the ratio between the surface return power in rain to that measured in adjacent rain free areas. Dual-polarized radar systems enable the use of differential phase measurements (Φ_{dp}) to estimate the total path attenuation. As matter of fact, scattering simulations have demonstrated (e.g., Bringi et al., 1990; Jameson, 1992), A_{hh} is linearly related to K_{dp}

$$A_{hh} = \gamma K_{dp} \qquad (A12)$$

and consequently

$$\int_{r_0}^{r_n} A_{hh}(s)\, ds = \gamma \int_{r_0}^{r_n} K_{dp}(s)\, ds$$
$$= \gamma\Big[\Phi_{dp}(r_n) - \Phi_{dp}(r_0)\Big] \qquad (A13)$$

The ZPHI method proposed in Testud et al. (2000) derives from the HB solution and coincides with CA when the condition (A12) is used to estimate the PIA.

In this approach the coefficient γ is assumed to be known though it depends on temperature (Jameson, 1992). This assumption leads to an improper estimation of the PIA affecting the attenuation correction procedure. To overcome this problem a self-consistent approach to optimize the Φ_{dp} constraint has been proposed in Bringi et al. (2001). This method also corrects the Z_{dr} profiles by assuming that A_{dp} is linearly related to A_{hh} and improving the constraint-based method proposed in Smyth and Illingworth (1998).

References

Abramowitz, M. and Stegun, I. A. (Eds.): Handbook of Mathematical Functions with Formulas, Graphs and Mathematical Tables, 9th printing, New York: Dover, 1972.

Andsager, K., Beard, K. V., and Laird, N. F.: Laboratory measurements of axis ratios for large rain drops, J. Atmos. Sci., 56, 2673–2683, 1999.

Atlas, D. and Ulbrich, C. W.: Path and area integrated rainfall measurement by microwave attenuation in the 1–3 cm band, J. Appl. Meteorol., 16, 1322–1331, 1977.

Beard, K. V. and Jameson, A. R.: Raindrop canting, J. Atmos. Sci., 40, 448–454, 1983.

Berenguer, M., Corral, C., Sánchez-Diezma, R., and Sempere-Torres, D.: Hydrological validation of a radar-based nowcasting technique, J. Hydrometeorol., 6, 532–549, 2005.

Berne, A., Delrieu, G., Creutin, J.-D., and Obled, C.: Temporal and spatial resolution of rainfall measurements required for urban hydrology, J. Hydrol., 299(3–4), 166–179, 2004.

Berne, A. and Uijlenhoet, R.: A stochastic model of range profiles of raindrop size distributions: Application to radar attenuation correction, Geophys. Res. Lett., 32, L10803, doi:10.1029/2004GL021899, 2005.

Bringi, V. N., Chandrasekar, V., Balakrishnan, N., and Zrnic, D. S.: An examination of propagation effects in rainfall on radar measurements at microwave frequencies, J. Atmos. Ocean. Technol., 7, 829–840, 1990.

Bringi, V. N., Keenan, T. D., and Chandrasekar, V.: Correcting C-band radar reflectivity and differential refelctivity data for rain at-

tenuation: a self-consistent method with constraints, IEEE Trans. Geosci. Remote Sensing, 39, 1906–1915, 2001.

Bringi, V. N. and Chandrasekar, V.: Polarimetric doppler weather radar, Cambridge University Press, 2001.

Chandrasekar, V. and Bringi, V. N.: Simulation of radar reflectivity and surface measurements of rainfall, J. Atmos. Oceanic Technol., 4, 464–478, 1987.

Chuang, C. and Beard, K. V.: A numerical model for the equilibrium shape of electrified raindrops, J. Atmos. Sci., 19, 1374–1389, 1990.

Collier, C. G. and Knowles, J. M.: Accuracy of rainfall estimates by radar, part III: application for short-term flood forecasting, J. Hydrol., 83, 237–249, 1986.

Gorgucci, E., Scarchilli, G., and Chandrasekar, V.: Error structrure of radar rainfall measurement at C-band frequencies with dual-polarization algorithm for attenuation correction, J. Geophys. Res., 101, 26 461–26 471, 1996.

Gorgucci, E., Scarchilli, G., and Chandrasekar, V.: A procedure to calibrate multiparameter weather radar using properties of the rain medium, IEEE Trans. Geosci. Remote Sens., 37, 269–276, 1999.

Haykin, S.: Neural networks: a comprehensive foundation, Mcmillan Coll., New York, NY, 1995.

Hitschfeld, W. and Bordan, J.: Errors inherent in the radar measurement of rainfall at attenuating wavelengths, J. Meteorol., 11, 58–67, 1954.

Hildebrand, P. H.: Iterative correction for attenuation of 5 cm radar in rain, J. Appl. Meteorol., 17, 508–514, 1978.

Iguchi, T. and Meneghini, R.: Intercomparisons of single-frequency methods for retrieving a vertical profile from airborne or space-borne radar data, J. Atmos. Oceanic Technol., 11, 1507–1516, 1994.

Illingworth, A. J. and Blackman, T. M.: The need to represent raindrop size spectra as normalized gamma distributions for the interpretation of polarization radar observations, J. Appl. Meteorol., 41, 1578–1590, 2002.

Jameson, A. R.: The effect of temperature on attenuation-correction schemes in rain using polarization propagation differential phase shift, J. Appl. Meteorol., 31, 1106-1118, 1992.

Le Bouar, E., Testud, J., and Keenan, T. D.: Validation of the rain profiling algorithm ZPHI from the C-band polarimetric weather radar in Darwin, J. Atmos. Ocean. Technol., 18, 1819–1837, 2001.

Lee, G. W., Zawadzki, I., Szyrmer, W., Sempere-Torres, D., and Uijlenhoet, R.: A general approach to double-moment normalization of drop size distributions, J. Appl. Meteorol., 43, 264–281, 2004.

Marzano, F. S., Picciotti, E., and Vulpiani, G.: Rain field and reflectivity vertical profile reconstruction from C-band radar volumetric data, IEEE Trans. Geosci. Rem. Sens., 42, 1033–1046, 2004.

Meneghini, R., Eckerman, J., and Atlas, D.: Determination of rain rate from space-borne radar using measurements of total attenuation, IEEE Trans. Geosci. Remote Sens., 21, 34–43, 1983.

Meneghini, R. and Nakamura, K.: Range profiling of the rain rate by an airborne weather radar, Remote Sens. Environ., 31, 193–209, 1990.

Meneghini, R., Kozu, T., Kumagai, H., and Boncyk, W. C.: A study of rain estimation methods from space using dual-wavelength radar measurements at near-nadir incidence over ocean, J. Atmos. Ocean. Technol., 9, 364–382, 1992.

Mishchenko, M. I.: Calculation of the amplitude matrix for a nonspherical particle in a fixed orientation, Appl. Opt., 39, 1026–1031, 2000.

Ray, P. S.: Broadband complex refractive indices of ice and water, Appl. Opt., 11, 1836–1844, 1972.

Scarchilli, G., Gorgucci, E., Chandrasekar, V., and Seliga, T. A.: Rainfall estimation using polarimetric techniques at C-band frequencies, J. Appl. Meteorol., 32, 1150–1160, 1993.

Seliga, T. A. and Bringi, V. N.: Potential use of radar differential reflectivity measurements at orthogonal polarizations for measuring precipitation, J. Appl. Meteorol., 15, 69–76, 1976.

Smyth T. J. and Illingworth, A. J.: Correction for attenuation of radar reflectivity using polarization data, Q. J. R. Meteorol. Soc., 124, 2393–2415, 1998.

Testud, J., Le Bouar, E., Obligis, E., and Ali-Mehenni, M.: The rain profiling algorithm applied to polarimetric weather radar, J. Atmos. Ocean. Technol., 17, 332–356, 2000.

Testud, J., Oury, S., Black, R. A., Amayenc, P., and Dou, X.: The concept of "normalized" distribution to describe raindrop spectra: A tool for cloud physics and cloud remote sensing, J. Appl. Meteorol., 40, 1118–1140, 2001.

Uijlenhoet, R., Andrieu, H., Austin, G., Baltas, E., Borga, M., Brilly, M., Cluckie, I., Creutin, J.-D., Delrieu, G., Deshons, P. , Fatorelli, S., Griffith, R., Guarnieri, P., Hang, D., Mimikou, M., Moani, M., Porrà, J., Sempere-Torres, D., and Spagni, D.: Integrated Radar Experiment (HIRE) : experimental setup and first results, in: 29th Int. Conf. On Radar Meteorology, AMS, 926–930, Montral, Canada, 1999.

Ulbrich, C. W.: Natural variations in the analytical form of the raindrop-size distribution, J. Climate Appl. Meteorol., 22, 1764–1775, 1983.

Willis, P. T.: Functional fit to some observed drop size distributions and parametrization of rain, J. Atmos. Sci., 41, 1648–1661, 1984.

Wyss, J., Williams, E. R., and Bras, R. L.: Hydrologic modeling of New England river basins using radar rainfall data, J. Geophys. Res., 95, 2143–2152, 1990.

Zrnić, D. S. and Ryzhkov, A.: Advantages of rain measurements using specific differential phase, J. Atmos. Ocean. Technol., 13, 454–464, 1996.